)evelopment 25:153.

iiths, J.F. 1998. Journal of the
tions 94:1725.

·uel 74(7):1083.

vanced Materials for Optics and

, R.D. Jr. 1960. SAE Technical

rmation Cirular 7474. US Bureau

ummer 1971; U.S. Department of
 Fuel Oils.

:chnical Paper Series 790922.
eries 841344.

5:37.

RA Journal of Research 7:47.

NUMERICAL MODEL FOR WAX DEPOSITION IN OIL WELLS

Edgar Ramirez-Jaramillo,[1] Carlos Lira-Galeana,[1,*]
and Octavio Manero Brito[2]

[1]Molecular Simulation Research Program, Mexican
Institute of Petroleum, Av. Eje Central Lazaro Cardenas
152, C.P. 07730, Mexico D.F., Mexico
[2]Department of Polymers, Materials Research Institute
(UNAM), Mexico D.F., 04510, Mexico

ABSTRACT

A liquid-solid compositional model that uses an equation of
state has been developed to predict the phenomenon of wax
deposition in model oil wells. Numerical solutions to the con-
servation equations for Newtonian-to-non-Newtonian flow
regimes show temperature, radial mass flux and wax deposition
profiles as a function of time and position in the pipe, using
realistic pressure and temperature profiles of a model well. Such
rheologic regime changes are dictated by thermodynamic
arguments.

*Corresponding author. E-mail: clira@imp.mx

www.dekker.com

INTRODUCTION

Deposition of solid organic materials in production facilities is a major problem of the oil industry, since the deposition of waxes (high molecular weight hydrocarbons) on production wells can cause serious economic loss due to the obstruction of the fluid flow systems. For this reason, the development of predictive models for wax deposition in those systems is of significant importance.

Most crude oils consist of various fractions of heavy hydrocarbons, which are known to precipitate as paraffin deposits due to either evaporation of volatile light ends (which otherwise act as naturally occurring solvents) or drop in the system temperature. Accumulation of these solids in transport pipes and process equipment is an old and expensive problem in the petroleum industry. This problem is expected to increase in the future as existing reserves are being depleted and offshore deep water explorations continue to grow.

The purpose of this work is to describe the relevant mechanisms of wax deposition from a waxy crude and to determine the expected composition and thickness of the deposits in a vertical pipe as the crude flows upwards as a function of time and position, using a novel approach based on thermodynamic arguments, the fluid flow conservation equations, and a model for the viscosity of the oil.

LITERATURE REVIEW

In a pioneering work, Burger et al. (1981), have investigated mechanisms of wax deposition. According to those authors, the deposition occurs on the pipe as a consequence of the transport of both dissolved and precipitated waxy crystals (the deposits of crude wax or paraffin that accumulate in flow lines, consists of very small wax crystals that tend to agglomerate and form granular particles of wax about the size of the grains of ordinary table salt, Reistle, 1932) when the flowing oil is cooling. The lateral transport of the waxy crystals is due to three mechanisms, diffusion, shear dispersion and Brownian diffusion. Molecular diffusion dominates at higher temperatures and heat flux conditions, whereas shear dispersion is the dominant mechanism at the lower temperatures and low heat fluxes. The contribution of Brownian diffusion is small compared with the other mechanisms. With these assumptions, a mechanistic model capable of calculating the expected wax deposition in pipeline systems was formulated.

There are approaches that deal with the so-called "particulate flow systems", consisting in solid particles which are already formed in the flow

ION

in production facilities is a major
osition of waxes (high molecular
: can cause serious economic loss
; systems. For this reason, the
deposition in those systems is of

ractions of heavy hydrocarbons,
araffin deposits due to either
ich otherwise act as naturally
i temperature. Accumulation of
)cess equipment is an old and
.try. This problem is expected to
are being depleted and offshore

ribe the relevant mechanisms of
nd to determine the expected
s in a vertical pipe as the crude
)osition, using a novel approach
uid flow conservation equations,

EVIEW

al. (1981), have investigated
to those authors, the deposition
the transport of both dissolved
ts of crude wax or paraffin that
small wax crystals that tend to
‾wax about the size of the grains
i the flowing oil is cooling. The
: to three mechanisms, diffusion,
√olecular diffusion dominates at
ons, whereas shear dispersion is‾
:ratures and low heat fluxes. The
mall compared with the other
mechanistic model capable of
pipeline systems was formulated.
i the so-called "particulate flow
h are already formed in the flow

and interact between themselves with no specific forces (Johansen, 1991). These pictures of liquid–solid flow are unable to describe the phenomenon of wax deposition, in which the solids are solely formed at the WAP (wax appearance point, i.e. the temperature in which wax begins to precipitate out) in the solid–liquid equilibrium envelope (Ferworn and Svrcek, 1998) and are transferred to the walls by radial diffusion.

Svendsen (1993) has presented a mathematical model of wax deposition in oil-pipeline system which takes into account the mechanisms mentioned above, i.e. thermodynamic equilibrium and diffusion of the solid species. Furthermore, the model takes into account the temperature profile along the pipe. This approach to the problem is used in the present work.

Fukui and Maeda (1998) carried out direct simulations of unsteady layer solidification for an eutectic binary fluid of lauric acid and myristic acid, which exhibits laminar flow between two parallel walls of different temperatures. Two-dimensional differential equations for momentum, heat and mass transfer were solved using finite differences. The predictions were discussed with reference to the time-changes of the shape of the solid–liquid (S–L) interface, the growth rate, the concentration at the (S–L) interface, the super-cooled layer adjacent to the S–L interface, and the component concentration in the solid phase.

More recently, Lindeloff (1999) developed a pipeline deposition mechanisms in which plug flow was assumed to simplify the problem, and this profile is not affected by the thickness of the deposited wax layer. Another assumption in this model is that the viscosity of the fluid is independent of both temperature and concentration of wax components, which of course is not real in practical applications.

This work presents a numerical solution to the radial mass flux using different velocity profiles (parabolic and plug) and explores the wax deposition behavior under those flow patterns. The flow model considers a multi-solid thermodynamic model where solid–liquid–vapor equilibrium is introduced (which will be described later in the paper), coupled to the equations of motion, energy and mass transfer. In the present work, results are presented for the simplified solid–liquid equilibrium approach in a two-component mixture.

NUMERICAL MODEL

System description. The fluid consists of n hydrocarbon components. For multi-component systems, the composition and mole fraction of the phases that coexist in thermodynamic equilibrium are functions of pressure and temperature. Therefore, in a compositional two-phase flow system

(liquid–solid), the composition of the phases changes along the pipe (Goyon et al., 1988).

Assumptions related to flow. Waxy oils are non-Newtonian fluids at temperatures below the WAP (wax appearance point) and Newtonian fluids otherwise (Wardhaugh and Borger, 1991). Since both viscosity and wax thickness may change along the pipeline, a turbulence contribution in the laminar sub-layer is possible, although it is assumed to be negligible. It is further assumed that the wax/oil boundary changes very slowly in the axial direction so that a quasi steady-state model is applicable for all rate processes concerning energy and mass. Heat associated with frictional heating, axial thermal diffusion and phase transitions are supposed to be negligible compared to heat convection.

The governing conservation equations for the mixture are:

$$\text{Mass:} \qquad \frac{\partial \rho_m}{\partial t} + \nabla \cdot \rho_m \underline{v} = 0 \qquad (1)$$

$$\text{Momentum:} \qquad \rho_m \left(\frac{\partial \underline{v}}{\partial t} + \underline{v} \cdot \nabla \underline{v} \right) = -\nabla p + \nabla \cdot \underline{\underline{\tau}} + \rho_m \underline{g} \qquad (2)$$

$$\text{Energy:} \qquad \rho_m C_v \left(\frac{\partial T}{\partial t} + \underline{v} \cdot \nabla T \right) = k \nabla^2 T \qquad (3)$$

where ρ_m and v are the mixture density and macroscopic velocity of the mixture.

p, τ and g are the pressure, stress tensor and gravitational constant, and C_v, k and T stand for the heat capacity, thermal conductivity and temperature, respectively.

The continuity equation for the liquid phase in the absence of source and sinks is:

$$\left(\frac{\partial \rho_L}{\partial t} \right) = -\nabla \cdot (\rho_L \underline{v} + \underline{J} \, \text{L}) \qquad (4)$$

where ρ_L and J_L are the liquid phase density and the mass flux of the liquid phase.

We assume that the fluid mixture is incompressible, i.e.:

$$\nabla \cdot \underline{v} = 0 \qquad (5)$$

ses changes along the pipe (Goyon

oils are non-Newtonian fluids at
arance point) and Newtonian fluids
91). Since both viscosity and wax
e, a turbulence contribution in the
it is assumed to be negligible. It is
ary changes very slowly in the axial
model is applicable for all rate
s. Heat associated with frictional
ase transitions are supposed to be

ions for the mixture are:

$$\nabla \cdot \rho_m \underline{v} = 0 \tag{1}$$

$$\left. \overline{v} \underline{v} \right) = -\nabla p + \nabla \cdot \underline{\underline{\tau}} + \rho_m \underline{g} \tag{2}$$

$$\left. + \underline{v} \cdot \nabla T \right) = k\nabla^2 T \tag{3}$$

ty and macroscopic velocity of the

s tensor and gravitational constant,
capacity, thermal conductivity and

iquid phase in the absence of source

$$(\rho_L \underline{v} + \underline{J} \, L) \tag{4}$$

e density and the mass flux of the

is incompressible, i.e.:

$$= 0 \tag{5}$$

and also quasi-steady state for all rate processes concerning mass, energy and momentum.

The constitutive equation for the fluid is the power-law model:

$$\underline{\underline{\tau}} = K\dot{\underline{\gamma}}^n \tag{6}$$

where K is the consistency index, γ is the shear rate and n is the power-law index.

The constitutive equation for the mass flux follows Fick's law:

$$\underline{J} = -D\nabla\rho_L \tag{7}$$

where D is the diffusion coefficient.

Solution of Eqs. (1), (2) and (6) for a pipe flow renders the following velocity profile:

$$v_z(r) = v_{max}\left[1 - \left(\frac{r}{R_w}\right)^{1+(1/n)}\right] \tag{8}$$

where

$$v_{max} = \frac{n\pi R_w}{1+3n}\left(\frac{R_w \Delta P}{2\eta L}\right)^{1/n} \tag{8a}$$

In Eq. (8a) R_w is the pipe radius minus the width of the deposited wax layer, η is the viscosity. $(\Delta P)/L$ is the pressure gradient which drives the flow.

The volumetric flow rate corresponding to Eq. (8) is:

$$Q = \frac{n\pi R_w^3}{1+3n}\left(\frac{R_w \Delta P}{2\eta L}\right)^{1/n} \tag{9}$$

For the system under consideration, Eq. (3) becomes:

$$v_z(r)\frac{\partial T}{\partial z} = \alpha\left(\frac{\partial^2 T}{\partial r^2} + \frac{1}{r}\frac{\partial T}{\partial r} + \frac{q_h}{k}\right) \tag{10}$$

where α is the thermal diffusivity of the fluid with thermal conductivity k and specific heat capacity C_p, and q_h is a heat source term associated with a phase transition from the liquid to the solid state. Equation (10) assumes that the thermal Peclet number P_{eT} (vR/α) is very large, which is the limit found in a real situation (Ribeiro et al., 1997).

The boundary conditions are:

$$T(r,0) = T_0 \quad 0 \leq r \leq R_0 \tag{11a}$$

$$T(0,z) = \text{finite} \quad z > 0 \tag{11b}$$

$$-k\frac{\partial T}{\partial r}\bigg|_{r=R_w} = h_{\text{Tot}}\Big[T(R_w, z) - T_\alpha(z)\Big] \tag{11c}$$

Equation (11) is the boundary condition corresponding to the cooling of the liquid due to the temperature gradient existing between the geothermal temperature of the rock in contact with the exterior pipe wall $T_\alpha(z)$ and the temperature of the liquid in contact with the deposited layer $T(R_w, z)$. The global heat transfer coefficient h_{Tot} is given as the sum of the resistances (in terms of the thickness Δ and thermal conductivities k) of the solid phases corresponding to the pipe wall, wax and the resistance due to the interface solid–liquid h_{film}^{-1}:

$$h_{\text{Tot}} = \frac{1}{R_w}\left(\frac{\Delta_{\text{pipe}}}{k_{\text{pipe}}} + \frac{\Delta_{\text{wax}}}{k_{\text{wax}}} + \frac{1}{h_{\text{film}}}\right)^{-1} \tag{12}$$

Equation (12) takes into account the variation of deposited layer thickness Δ_{wax} and therefore the global heat transfer coefficient changes with axial distance.

Considering the quasi steady-state condition, Eq. (4) may be expressed as:

$$v_z(r)\frac{\partial \rho_L}{\partial z} = -\left[\frac{1}{r}\frac{\partial}{\partial r}(rJ_r) + \frac{\partial}{\partial z}J_z\right] \tag{13}$$

where $v_z(r)$ is given by Eq. (8) and J_r and J_z are the mass flux components. In the actual situation, the mass Peclet number $v_z R/D$ for this type of flow is very large, so we consider $v_z(r)(\partial \rho_L/\partial z) \gg (\partial J_z/\partial z)$, i.e. axial convection dominates over axial diffusion. Equation (7) becomes:

$$J_r = -D\frac{\partial \rho_L}{\partial r} \tag{14}$$

In the problem under consideration, the mass density of the liquid phase is a function of the temperature and pressure (described through an equation of state). Since temperature is a function of position in space, i.e. of r and z, then:

$$\frac{\partial \rho_L[T(r,z)]}{\partial r} = \left(\frac{\partial \rho_L}{\partial T}\right)\frac{\partial T(r,z)}{\partial r} \tag{15}$$

$\} \leq r \leq R_o$ (11a)

$z > 0$ (11b)

$T(R_w, z) - T_\alpha(z)\Big]$ (11c)

ndition corresponding to the cooling
ure gradient existing between the
contact with the exterior pipe wall
d in contact with the deposited layer
ficient h_{Tot} is given as the sum of the
and thermal conductivities k) of the
wall, wax and the resistance due to

$\Big| \dfrac{\Delta_{\text{wax}}}{k_{\text{wax}}} + \dfrac{1}{h_{\text{film}}}\Big)^{-1}$ (12)

int the variation of deposited layer
bal heat transfer coefficient changes

ite condition, Eq. (4) may be expres-

$\dfrac{\partial}{\partial r}(rJ_r) + \dfrac{\partial}{\partial z}J_z\Big]$ (13)

id J_z are the mass flux components. In
number $v_z R/D$ for this type of flow is
$/\partial z) \gg (\partial J_z/\partial z)$, i.e. axial convection
ion (7) becomes:

$D\dfrac{\partial \rho_L}{\partial r}$ (14)

ation, the mass density of the liquid
e and pressure (described through an
s a function of position in space, i.e. of

$\Big(\dfrac{\partial \rho_L}{\partial T}\Big)\dfrac{\partial T(r, z)}{\partial r}$ (15)

Substitution of (15) into (13) and (14) leads to:

$$J_r = -D\Big(\frac{\partial \rho_L}{\partial T}\Big)\frac{\partial T}{\partial r} \tag{16}$$

$$v_z(r)\frac{\partial \rho_L}{\partial z} = \frac{1}{r}\frac{\partial}{\partial r}Dr\Big(\frac{\partial \rho_L}{\partial T}\Big)\frac{\partial T}{\partial r} \tag{17}$$

Similarly, the conservation equation for the solid phase is:

$$v_z(r)\frac{\partial \rho_S}{\partial z} = \frac{1}{r}\frac{\partial}{\partial r}Dr\Big(\frac{\partial \rho_S}{\partial r}\Big) \tag{18}$$

Equations (17) or (18), may be solved under the following boundary conditions:

$$\rho_L = \rho_L^o \quad \text{at } z = 0 \tag{18a}$$

$$\rho_L = \text{finite} \quad \text{at } r = 0 \tag{18b}$$

$$\rho_L = \rho_{Lw} \quad \text{at } r = R_w \tag{18c}$$

and same expressions for the solid densities. Densities at $z = 0$ and at $r = R_w$ follow the thermodynamic equilibrium given T and P at the pipe entrance and at the solid–liquid interface, respectively, as considered in what follows.

To calculate the variation of the density of the liquid phase as a function of temperature (and pressure), an equation of state is needed. In this work, liquid as solid-phase properties are calculated through an equation of state. The thermodynamics of this problem is based on the experimental supported assumption that wax precipitation is a multi-solid-phase precipitation process (Lira-Galeana et al., 1996). The number and identity of the phases that precipitate from a liquid hydrocarbon mixture can be determined by the following stability test:

$$f_i\Big(P, T, \underline{z}\Big) - f_{\text{pure},i}^S(P, T) \geq 0 \quad i = 1, 2, \ldots, N \tag{19}$$

In this framework each solid phase is described as a pure component that does not mix with other solid phases. This approach suggests that large hydrocarbons are mutually insoluble in the solid state, contrary to those methods based on regular solution theory of mixtures or on equilibrium of state, which assume that all the components that precipitate from the liquid or vapor form a solid solution (Won, 1989).

Since the thermodynamic equilibrium requires that the fugacity of each component in the liquid phase is equal to the fugacity of the pure

components in the solid phase, it is required that $\partial \rho_L / \partial T$ be expressed in terms of the solid fractions. The mass density of the mixture is given by:

$$\rho_m = \rho_L + \rho_S \tag{20}$$

The total weight fractions of liquid and solid in the mixture are:

$$w_x = \frac{\rho_L}{\rho_m} \quad \text{and} \quad w_S = \frac{\rho_S}{\rho_m} \tag{21}$$

and hence

$$\frac{\partial \rho_L}{\partial T} = -\rho_m \frac{\partial w_S}{\partial T} + (1 - w_S) \frac{\partial \rho_m}{\partial T} \tag{22}$$

Then the radial mass flux is the sum of the contributions of flux of each component in the mixture, i.e.:

$$J_{ri} = -D\left[\left(-\rho_m \frac{\partial w_{si}}{\partial T} + (1 - w_{si}) \frac{\partial \rho_m}{\partial T}\right)\left(\frac{\partial T}{\partial r}\right)\right] \tag{23}$$

$$J_r = \sum_{i=1}^{N} J_{ri} \tag{24}$$

where w_{Si} is the solid fraction of the ith component in the solid phase.

The total amount of deposited mass at time t and distance from inlet (i.e. from bottom to the surface) z is expressed as Svendsen (1993):

$$M(t, z) = \sum_{i=1}^{N} M_i(t, z) = \sum_{i=1}^{N} 2\pi \int_0^t \int_0^z R_w J_{ri}|_{r=R_w} \, dz \, dt \tag{25}$$

where the mass flux (Eq. (23)) is evaluated at the liquid–solid interface ($r = R_w$).

The derivative of M is:

$$\frac{\partial M}{\partial z} = \pi(R_o^2 - R_w^2)\rho_S = \sum_{i=1}^{N} \frac{\partial M_i}{\partial z} = \sum_{i=1}^{N} 2\pi \int_0^t R_w J_{ri}|_{r=R_w} \, dt \tag{26}$$

Equation (26) is an implicit equation for R_w. Having found R_w, the total deposition rate is:

$$\frac{dM}{dt} = \sum_{i=1}^{N} \frac{dM_i}{dt} = \sum_{i=1}^{N} 2\pi \int_0^L R_w J_{ri}|_{r=R_w} \, dz \tag{27}$$

equired that $\partial \rho_L / \partial T$ be expressed in
density of the mixture is given by:

$$_L + \rho_S \qquad (20)$$

uid and solid in the mixture are:

$$w_S = \frac{\rho_S}{\rho_m} \qquad (21)$$

$$+ (1 - w_S) \frac{\partial \rho_m}{\partial T} \qquad (22)$$

: sum of the contributions of flux of

$$(1 - w_{si}) \frac{\partial \rho_m}{\partial T} \Big) \Big(\frac{\partial T}{\partial r} \Big) \Big] \qquad (23)$$

$$(24)$$

i th component in the solid phase.
nass at time t and distance from inlet
expressed as Svendsen (1993):

$$\sum_{i=1}^{N} 2\pi \int_0^t \int_0^z R_w J_{ri}|_{r=R_w} \, dz \, dt \qquad (25)$$

valuated at the liquid–solid interface

$$\frac{\partial M_i}{\partial z} = \sum_{i=1}^{N} 2\pi \int_0^t R_w J_{ri}|_{r=R_w} \, dt \qquad (26)$$

uation for R_w. Having found R_w, the

$$\cdot \sum_{1}^{N} 2\pi \int_0^L R_w J_{ri}|_{r=R_w} \, dz \qquad (27)$$

The average diffusion constant may be expressed as, Burger et al. (1981):

$$D = \frac{C_1}{\eta} \qquad (28)$$

where the viscosity η is a function of pressure and temperature taken from Werner et al. (1998):

$$\eta(P, T) = \left(\frac{\Psi + P}{\Psi + P_o} \right) \eta(P_o, T) \exp\left[\beta \left(\frac{1}{T} - \frac{1}{T_o} \right) \right] \qquad (29)$$

where β is a function of the viscosity at P_o and T_o, while Ψ is a parameter which is a function of the viscosity at the current temperature of the mixture. Equation (29) is also used to obtain the variation with temperature and pressure of the factor K in Eqs. (8a) and (9).

RESULTS AND DISCUSSION

Let us consider a model system with two representative crude oil components of different molecular weight, with weight fraction given by w_1 and w_2, and with typical values of geometry and flow rate. These are given in Table 1.

The calculations are performed from the bottom of a model oil well up to the surface of it. Given a geothermal axial temperature profile, the heat flow is transferred across the pipe wall, so that the liquid temperature diminishes along the pipe from bottom to surface conditions. Starting from T_o and P_o (temperature and pressure at the bottom of the reservoir), an initial guess of the pressure is used at each grid point (r, z). From Eqs. (8),

Table 1. Model Parameters and Input Information

Model Parameters (Units)	Values
Pipe radius, R_o (m)	0.15
Pipe length, L (m)	7364.7
Volumetric flow rate, Q (m³/h)	500
Molecular weight, PM_1 (Kg/Kmol)	222
Molecular weight, PM_2 (Kg/Kmol)	580
Tube inlet temperature T_o (K)	434
Weight fraction W_1	0.85
Weight fraction W_2	0.15

(8a) and (10), the new temperature profile is calculated. In Eq. (8), we consider parabolic flow and plug flow, i.e. $n = 1$ and $v_z = v_{max}$, respectively. Given the new values of pressure and temperature, the thermodynamic equilibrium (19) renders the solid and liquid fractions at these conditions. From the resulting fractions and the calculated temperature gradient, the mass flux may be evaluated at the wall (Eqs. (23) and (24)) calculating the diffusion coefficient through Eqs. (28) and (29). Equation (27) provides the deposition rate, which is a function of the mass flux and R_w, the latter is found using Eq. (26). It is necessary to mention that only the solid fractions that are next to the wall are those which may be deposited, since the deposition rate expression (Eq. (27)) considers the mass flux evaluated at the solid–liquid interface. Another important aspect to be considered is the fact that the solid and liquid fractions that are obtained through the thermodynamic equilibrium must satisfy the mass conservation Eqs. (17) and (18). Since the liquid and solid fractions profiles were obtained from the temperature profile Eq. (10), which is of the same form as Eqs. (17) and (18), it is expected that these profiles satisfy the conservation equations. We have verified Eq. (17) and (18) numerically with good agreement.

For the initial guess, the pressure gradient may be assumed linear, and a local mass balance is required to check the assumed pressure. This local mass balance may be expressed as follows:

$$(\rho_m)_i Q_i = (\rho_m)_{i+1} Q_{i+1} + \text{deposited mass} \qquad (30)$$

In Eq. (30), the volumetric flow rate Q is given by Eq. (9), where η follows the variation with temperature and pressure expressed in Eq. (29). The pressure value is updated to calculate the next temperature profile. The iterative process is repeated until the conditions at the surface are satisfied. A flow-chart that shows the procedure by which calculations are carried out throughout the geometry is depicted in appendix I. In Appendix II, the numerical method used in the solution of the convection-diffusion Eqs. (10), (17) and (18) is outlined.

In Figure 1, the calculated axial temperature profile of the bulk fluid and the geothermal axial temperature profile of the rock in contact with the exterior wall of the pipe, taken from hypothetical well data, is shown. The geothermal temperature decreases from 440 K to around 400 K almost linearly and during the last 2000 m temperature decreases more steeply to 310 K. The calculated temperature profile of the bulk fluid maintains a 10 degrees difference with the exterior temperature in most of the pipe length (from bottom to 2000 m). During the final 2000 m this difference decreases progressively and reduces to zero difference during the last 1500 m. The larger difference between both profiles in the interval 7365–6000 m

rofile is calculated. In Eq. (8), we
i.e. $n = 1$ and $v_z = v_{max}$, respectively.
d temperature, the thermodynamic
liquid fractions at these conditions.
alculated temperature gradient, the
all (Eqs. (23) and (24)) calculating
?8) and (29). Equation (27) provides
of the mass flux and R_w, the latter is
mention that only the solid fractions
which may be deposited, since the
nsiders the mass flux evaluated at the
nt aspect to be considered is the fact
; that are obtained through the
sfy the mass conservation Eqs. (17)
tions profiles were obtained from the
 the same form as Eqs. (17) and (18),
the conservation equations. We have
with good agreement.
gradient may be assumed linear, and
ck the assumed pressure. This local
ows:

$$\text{l + deposited mass} \tag{30}$$

rate Q is given by Eq. (9), where η
. and pressure expressed in Eq. (29).
ate the next temperature profile. The
onditions at the surface are satisfied.
by which calculations are carried out
in appendix I. In Appendix II, the
of the convection-diffusion Eqs. (10),

temperature profile of the bulk fluid
 profile of the rock in contact with
om hypothetical well data, is shown.
 from 440 K to around 400 K almost
uperature decreases more steeply to
 ofile of the bulk fluid maintains a
emperature in most of the pipe length
final 2000 m this difference decreases
difference during the last 1500 m.
rofiles in the interval 7365–6000 m
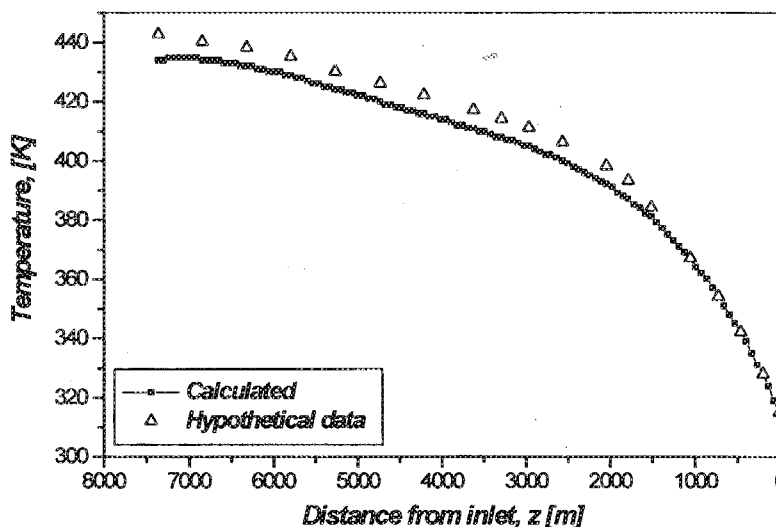
Figure 1. Geothermal axial temperature profile and calculated temperature of the bulk fluid.

reflects the larger driving force, which induces large deposition of the solid fractions within the region near to the bottom of the well.

Figure 2 depicts the measured pressure profile along the well from hypothetical data and the calculated pressure axial profile. Pressure decreases almost linearly from around 730 bar at the bottom of the well to approximately 138 bar at ground conditions. These pressure values are considered in the calculation of the thermodynamic equilibrium at each axial grid point, since no radial variation of the pressure is taken into account. Furthermore, these profiles confirm that the guessed values assuming a linear variation of pressure with distance are real.

Figure 3 shows the calculated radial temperature profile of the fluid at a point located near the bottom of the well, for the parabolic and plug-flow cases. This profile is obtained straightforwardly from the finite difference solution of Eq. (7). As observed, the plug flow temperature profile shows a larger temperature gradient close to the wall. It is interesting to note that the radial variation of temperature amounts to less than one degree. In fact, it is almost a flat temperature profile for both plug and Newtonian flows. This reflects the predominance of convection over diffusion in the energy equation, since according to data shown in Table 1, the Peclet number for this example is very large ($\sim 10^{12}$).
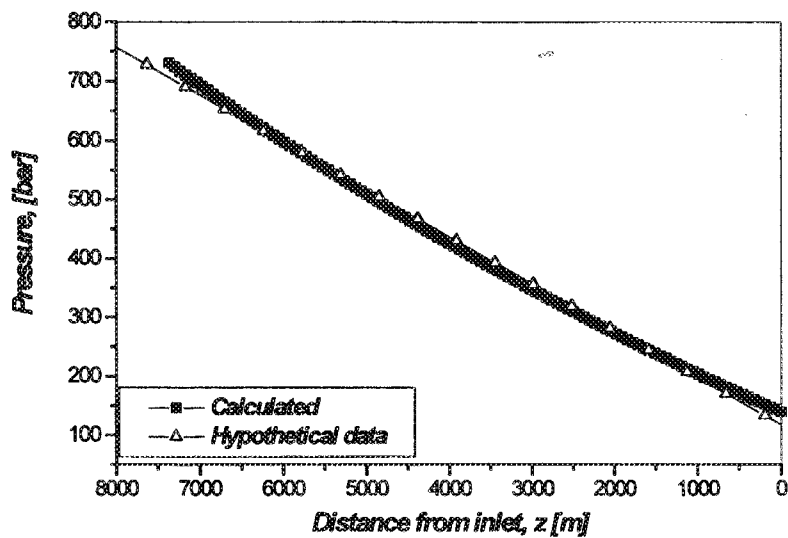
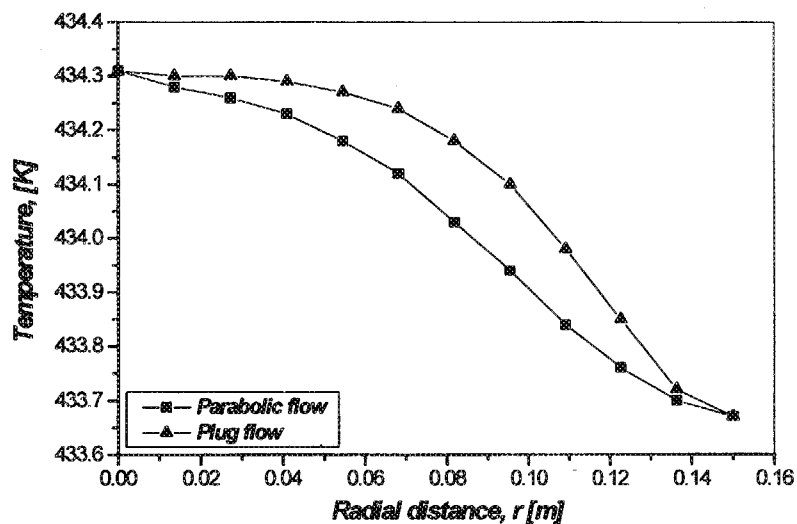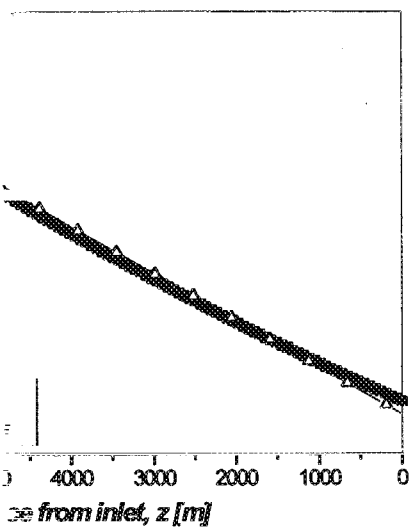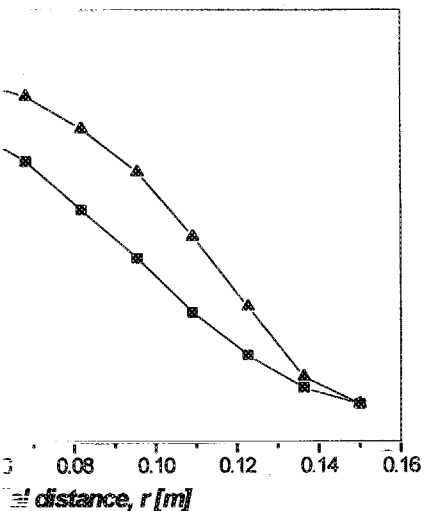*Figure 2.* Calculated and measured pressure profile.

Figure 3. Calculated radial temperature profile at $z = 7364.7$ m for parabolic and plug flow.

The total radial mass flux and that of the components of the precipitated solid phase are shown in Figure 4 for the case of parabolic flow (a) and plug flow, (b) as functions of the radial distance. The wall is located at $0.15\,\mathrm{m}$. J_1 is the mass flux of the light component (molecular weight $= 222$) and J_2 is that of the heavy component (molecular weight $= 580$). It is interesting to observe that the magnitude of the total mass flux is equal to the flux of the heavy component, i.e. the light component can not solidify under the given conditions of this hypothetical well, therefore its flux is zero. This is observed for both flows. Due to differences in the temperature gradients at the wall for plug and parabolic flows (see Figure 3), Eq. (23) leads to a larger radial mass flux in the case of plug flow. At the wall, differences amount to around 50% in the magnitude of the fluxes. Moreover, there are qualitative differences, since the parabolic flow mass flux presents a maximum located at $0.12\,\mathrm{m}$, but the mass flux in the plug flow shows a maximum located at the wall.

The radial mass flux increases substantially in regions close to the wall in the plug flow case, where the temperature gradient reaches a maximum. This is expected, since according to Eq. (23) the temperature gradient provides the driving force for radial diffusion mass flux.

4000   3000   2000   1000   0

:e from inlet, z [m]

id measured pressure profile.

0   0.08   0.10   0.12   0.14   0.16

=! distance, r [m]

ire profile at $z = 7364.7\,\mathrm{m}$ for parabolic and
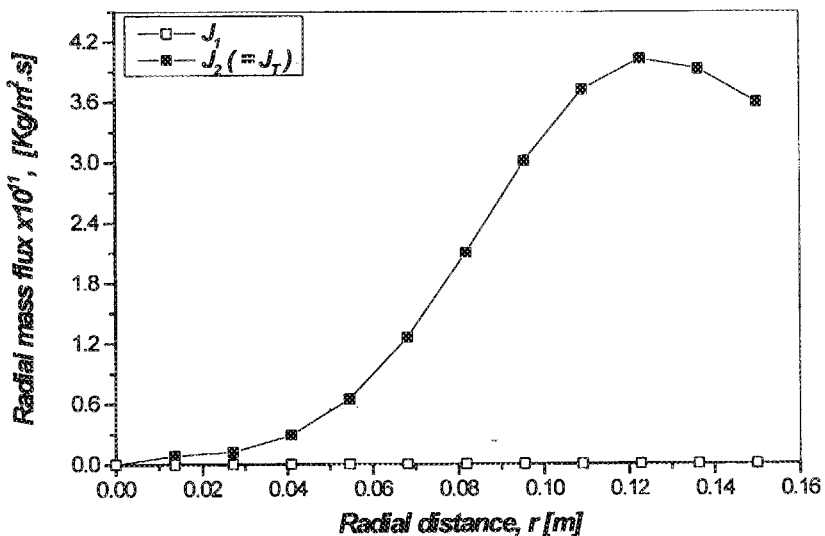
Figure 4a. Radial mass fluxes at $z = 3682.3\,\mathrm{m}$ for parabolic flow. J_1 (molecular weight $= 222$) and J_2 (molecular weight $= 580$) are the light and heavy components, respectively, and J_T is the total mass flux.
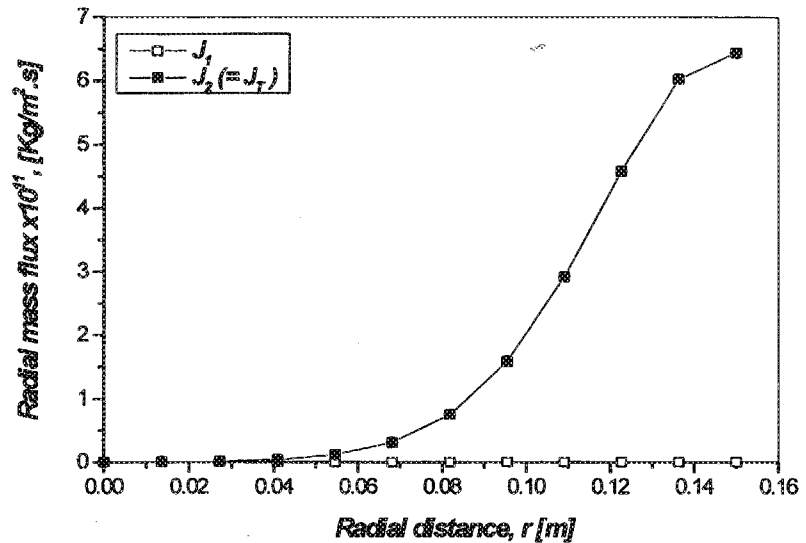
Figure 4b. Radial mass fluxes at $z = 3682.3\,\text{m}$ for plug flow. J_1 (molecular weight $= 222$) and J_2 (molecular weight $= 580$) are the light and heavy components, respectively, and J_T is the total mass flux.

It is possible to obtain the mass per unit volume of wax deposited on the pipe wall using Eq. (25). Results are plotted in Figure 5, where the mass deposited is given as a function of time for a fixed well depth (3945 m). As shown, only the heavy component give contribution to the wax deposited. The deposition rate (slope of the curves in Figure 5) increases for larger times. Past 111 hours, the deposited mass profile of components 1 and 2 in the mixture with distance from the bottom of the well is plotted in Figures 6a and 6b, for the parabolic and plug flows, respectively. The mass deposited per squared meter of heavy component is almost the same for both flows and the total mass deposited decreases from bottom to top of the well. Parabolic flow induces a steeper variation of the deposited mass in the region near to the bottom of the well, than in the case of plug flow. In the latter case, the total deposited mass decreases very slowly with distance, and drops steeply during the last 200 m from the ground.

The thickness of the deposited layer, calculated from $h(z, t) = R_o - R_w$, is plotted with the well depth in Figure 7a. Observe that an abrupt decrease in the wall thickness occurs between 500–1500 m from inlet. This is also noticeable in Figures 6a for the parabolic flow. The sudden increase in the wall thickness is partly due to the increase in temperature difference between the temperature of the well's wall and that of the liquid. In Figure 7b,

$= 3682.3$ m for plug flow. J_1 (molecular $= 580$) are the light and heavy components, ix.
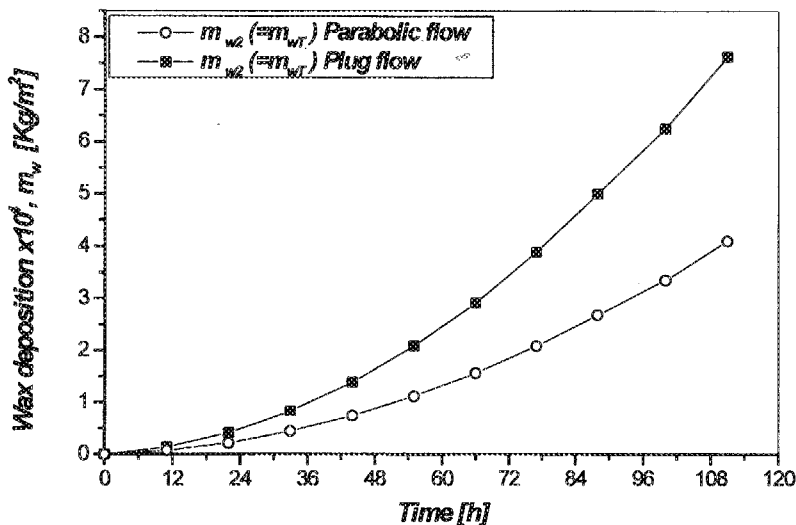

Figure 5. Total mass deposited as a function of time at $z = 7364.7$ m. Parabolic and plug flow. (1) Corresponds to the light component (molecular weight $= 222$), (2) corresponds to the heavy component (molecular weight $= 580$) and (T) is the total mass.
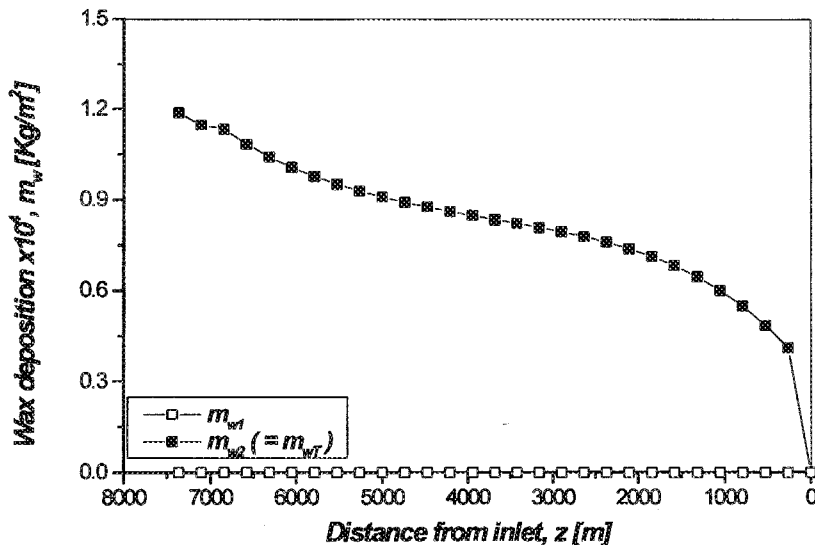
ss per unit volume of wax deposited on are plotted in Figure 5, where the mass ime for a fixed well depth (3945 m). As give contribution to the wax deposited. urves in Figure 5) increases for larger mass profile of components 1 and 2 in bottom of the well is plotted in Figures ; flows, respectively. The mass deposited nent is almost the same for both flows ases from bottom to top of the well. ariation of the deposited mass in the well, than in the case of plug flow. In mass decreases very slowly with dis- last 200 m from the ground.

layer, calculated from $h(z, t) = R_o - R_w$, ure 7a. Observe that an abrupt decrease n 500–1500 m from inlet. This is also abolic flow. The sudden increase in the rease in temperature difference between and that of the liquid. In Figure 7b,

Figure 6a. Wax deposition per m^2 of clean wall after 111 hr of flow. Parabolic flow. Same cases as in Figure 5.
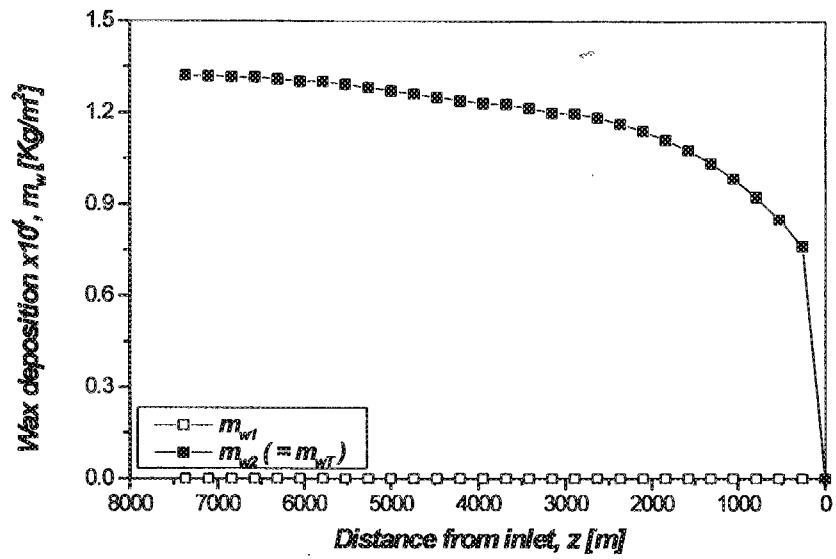
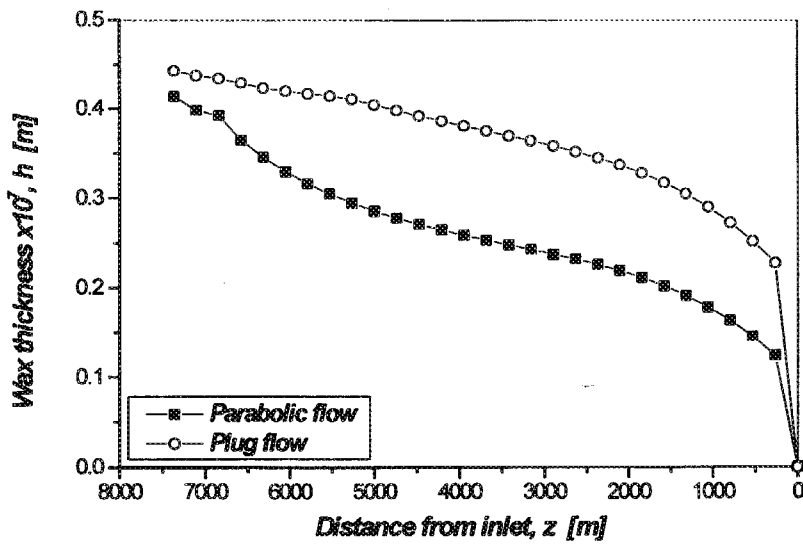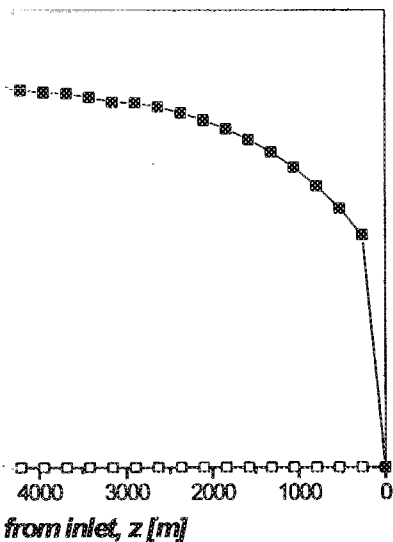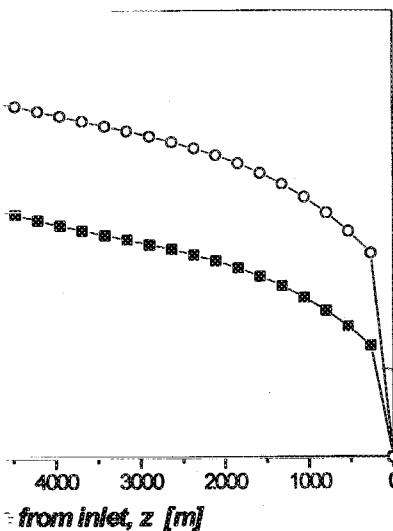**Figure 6b.** Wax deposition per m^2 of clean wall after 111 hr of flow. Plug flow. Same cases as in Figure 5.

Figure 7a. Wax thickness as a function of well depth for parabolic and plug flow.
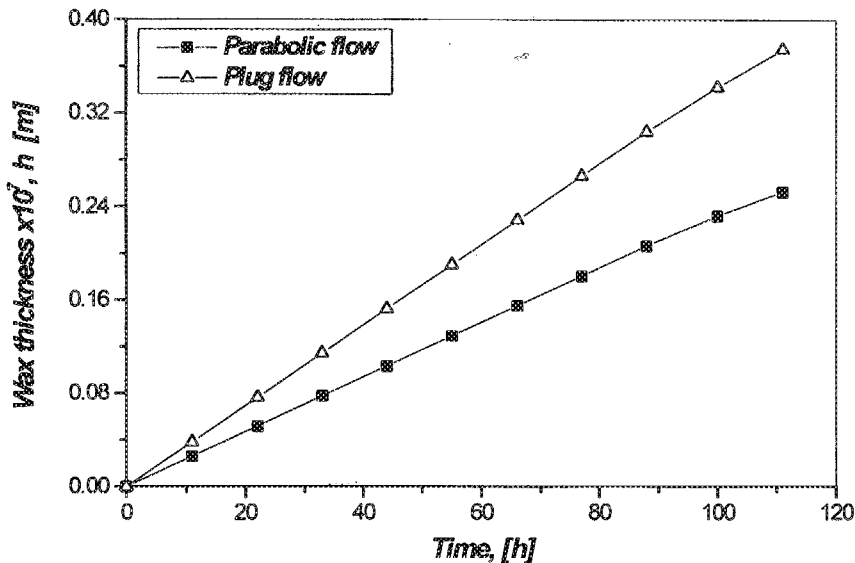
ean wall after 111 hr of flow. Plug flow.

Figure 7b. Wax thickness as a function of time at $z = 3682.3$ m for parabolic and plug flow.

is shown the thickness of the deposited layer as a function of time after 111 hours for both flows.

Finally, it is interesting to observe quantitative differences between results presented for parabolic flow and plug flow with regard to radial mass flux, mass deposited with time and wax deposited versus distance from inlet. This fact has important consequences if a parabolic (Newtonian) velocity profile is assumed for the entire geometry. As mentioned, waxy oils are non-Newtonian fluids at temperatures below the wax appearance point and Newtonian fluids otherwise. It is possible that fluid temperature may drop below the wax appearance point in some region of the well. This will induce a change in the rheological behavior of the fluid, adopting a near plug flow velocity profile. As mentioned, the plug flow will increase the rate of deposition of solids on the walls.

CONCLUSIONS

Wax deposition has been modeled by a model of a two component mixture in liquid–solid equilibrium undergoing plug and parabolic flows. Hypothetical field data of the fluid temperature and pressure along the

f well depth for parabolic and plug flow.

length of a typical inshore well and geothermal data are considered in the radial diffusion calculations. Results show that the deposited layer contains only amounts of heavy component, as this is predicted as a function of time and distance from the inlet. Quantitative differences with regard to the magnitude of the radial mass flux, solids deposition rates and mass deposited as a function of distance from inlet and time are observed in plug and parabolic flows. An extension to incorporate a full non-Newtonian behavior with shear rate and composition-dependent viscosity in a two-phase L-S multi-component mixture is currently under consideration.

APPENDIX I. THE FLOW CHART CALCULATION PROCEDURE
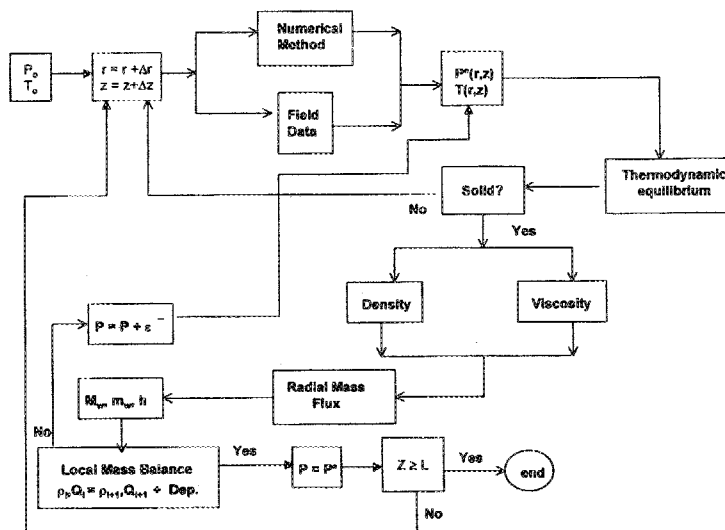
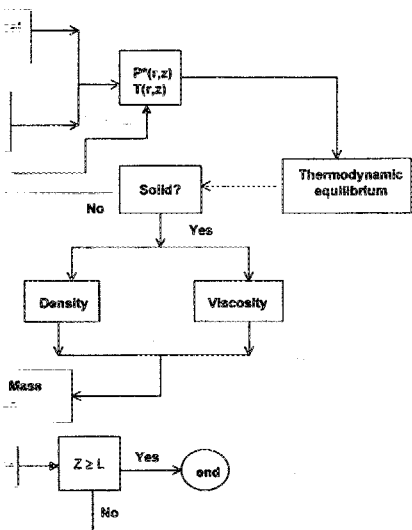## APPENDIX II. NUMERICAL METHOD

Using forward finite differences, the solution of Eq. (10), with $q_h = 0$, is written in dimensionless form as:

Plug flow

$$\frac{\partial \theta}{\partial \phi} = \left(\frac{\partial^2 \theta}{\partial \gamma^2} + \frac{1}{\gamma} \frac{\partial \theta}{\partial \gamma} \right) \tag{II.1}$$

d geothermal data are considered in the
is show that the deposited layer contains
, as this is predicted as a function of time
ntitative differences with regard to the
solids deposition rates and mass depo-
inlet and time are observed in plug and
corporate a full non-Newtonian behavior
dependent viscosity in a two-phase L-S
tly under consideration.

OW CHART CALCULATION
CEDURE

UMERICAL METHOD

es, the solution of Eq. (10), with $q_h = 0$, is

$$\left(\frac{\partial^2 \theta}{\partial \gamma^2} + \frac{1}{\gamma}\frac{\partial \theta}{\partial \gamma}\right)$$ (II.1)

Parabolic flow

$$(1 - \gamma^2)\frac{\partial \theta}{\partial \phi} = \left(\frac{\partial^2 \theta}{\partial \gamma^2} + \frac{1}{\gamma}\frac{\partial \theta}{\partial \gamma}\right)$$ (II.2)

where

$$\theta = \frac{T - T_o}{q_1(z)(R/k)} \qquad \gamma = \frac{r}{R} \qquad \phi = \frac{zk}{\rho C_p v_{max} R^2}$$

The forward finite difference formulation of the above equations is defined as:

$$\frac{\partial \theta}{\partial \phi} = \frac{\theta_{i,j+1} - \theta_{i,j}}{\Delta \phi}$$

$$\frac{\partial \theta}{\partial \gamma} = \frac{\theta_{i+1,j} - \theta_{i,j}}{\Delta \gamma}$$ (II.3)

$$\frac{\partial^2 \theta}{\partial \gamma^2} = \frac{\theta_{i+1,j} - 2\theta_{i,j} + \theta_{i-1,j}}{(\Delta \gamma)^2}.$$

Substituting Eq. (II.3) into Eqs. (II.1) and (II.2) gives:

Plug flow

$$\theta_{i,j+1} = \theta_{i,j} + \lambda\left[\theta_{i+1,j}\left(1 + \frac{1}{i}\right) - \theta_{i,j}\left(2 + \frac{1}{i}\right) + \theta_{i-1,j}\right]$$ (II.4)

Parabolic flow

$$\theta_{i,j+1} = \theta_{i,j} + \frac{\lambda}{1 - (i\Delta\gamma)^2}\left[\theta_{i+1,j}\left(1 + \frac{1}{i}\right) - \theta_{i,j}\left(2 + \frac{1}{i}\right) + \theta_{i-1,j}\right]$$ (II.5)

where

$$\lambda = \frac{\Delta \phi}{(\Delta \gamma)^2}$$ (II.6)

with the following boundary conditions:

$$\phi = 0 \quad \theta = 0$$ (II.7)

$$\gamma = 0 \quad \theta = \text{finite}$$ (II.8)

$$\gamma = 1 \quad \frac{\partial \theta}{\partial \gamma} = -1$$ (II.9)
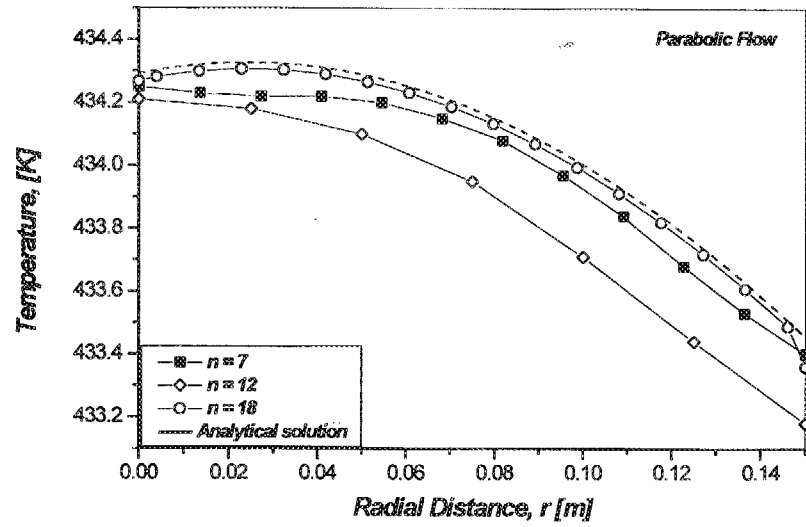
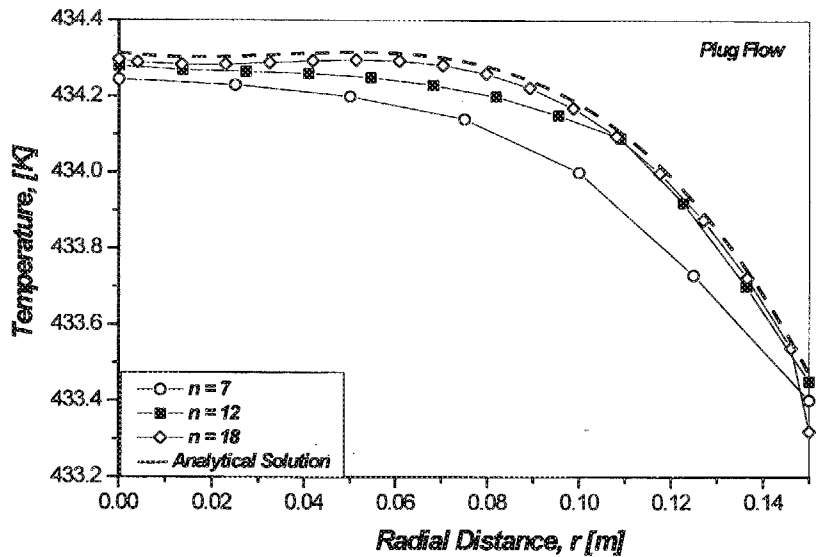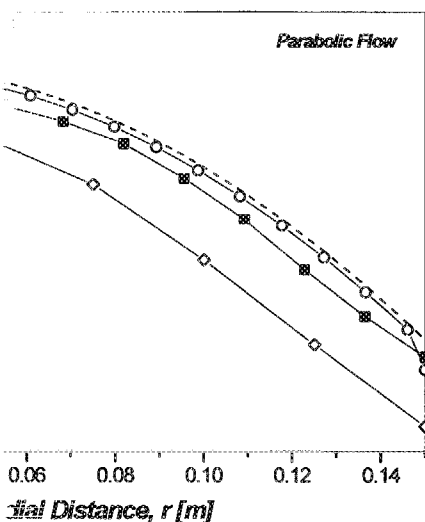*Figure 8a.* Comparison between analytical and numerical solutions for the heat Eq. (10). Parabolic flow.

Figure 8b. Comparison between analytical and numerical solutions for the heat Eq. (10). Plug flow.
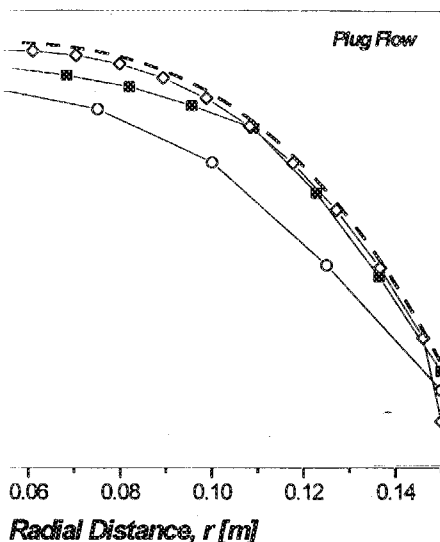
Figures 8a and 8b show comparisons between the numerical solution for the cases of parabolic and plug flow with the available analytical solutions (Schenk and Van Laar, 1958).

Parabolic Flow

lytical and numerical solutions for the heat

Plug Flow

Radial Distance, r [m]

lytical and numerical solutions for the heat

ACKNOWLEDGMENTS

REFERENCES

Burger, E.D., Perkins, T.K. and Striegler, J.H. 1981. "Studies of Wax Deposition in the Trans Alaska Pipeline", J. of Petroleum Technology 1075–1086.

Ferworn, K.A. and Svcrek, W.Y. 1998. "Characterization and Phase Behavior of Asphaltenic Crude Oils", in Structures and Dynamics of Asphaltenes, edited by Oliver C. Mullins and Eric Y. Sheu, Plenum Press: Chapter VII, 227–246.

Fukui, K. and Kouji Maeda. 1998. "Numerical Simulation of Dynamic Layer Solidification for a Eutectic Binary System", J. of Chem. Eng. of Japan Vol. 31, No. 2, 445–450.

Goyon, J.C., Shoham, O. and Brill, J.P. 1988. "Analysis of Computational Procedures for Multicomponent Flow in Pipelines," SPE 17573 219–232.

Johansen, S.T. 1991. "The Deposition of Particles on Vertical Walls", J. Multiphase Flow Vol. 17, No. 3, 355–376.

Lindeloff, N. 1999. "Formation of Solid Phases in Hydrocarbon Mixtures", Ph.D. Thesis, Department of Chemical Engineering, Technical University of Denmark, Chapter II, 4–6.

Lira-Galeana, C., Firoozabadi, A. and Prausnitz, J.M. 1996. "Thermo-dynamics of Wax Precipitation in Petroleum Mixtures", AIChE J. Vol 42, No. 1, 239.

Ribeiro, F.S., Souza Mendez, P.R. and Braga, S.L. 1997. "Obstruction of Pipelines Due to Paraffin Deposition During the Flow of Crude Oils". Int. J. Heat Mass Transfer 1–10.

Schenk, J. and van Laar, J 1958. "Heat Transfer in Non-Newtonian Laminar Flow in Tubes", Appl. Sci. Res. Section A Vol. 7, 449–462.

Svendsen, J.A. 1993. "Mathematical Modeling of Wax Deposition in Oil Pipeline Systems", AIChE J. Vol. 39, No. 8, 1377–1388.

Wardhaugh, L.T. and Borger, D.V. 1991. "Flow Characterization of Waxy Crude Oils: Application to Pipeline Design", AIChE J. 37(6):871.

Werner, A., De Hemptinne, J.C., Behar, F., Behar, E. and Boned, C. 1998. "A New Viscosity Model for Petroleum Fluids with High Asphaltenes Content", Fluid Phase Eq. 147:319–341.

Won, K.W. 1989. "Thermodynamic Calculation of Cloud Point Temperatures of Refined Hydrocarbon Mixtures", Fluid Phase Equilibria 53: 377–396.